Partitioning CO_2 net ecosystem exchange fluxes on the microsite scale in the Lena River Delta, Siberia

Tim Eckhardt[1,2], Christian Knoblauch[1,2], Lars Kutzbach[1,2], Gillian Simpson[3], Evgeny Abakumov[4] and Eva-Maria Pfeiffer[1,2]

[1]Institute of Soil Science, Universität Hamburg, Allende-Platz 2 Hamburg, 20146, Germany
[2]Center for Earth System Research and Sustainability, Universität Hamburg, Allende-Platz 2, Hamburg, 20146, Germany
[3]School of GeoSciences, University of Edinburgh, West Mains Road, Edinburgh, EH9 3JN, Scotland, UK
[4]Department of Applied Ecology, Saint-Petersburg State University, 199178, 16-line 2, Vasilyevskiy Island, Russia

Correspondence to: Tim Eckhardt (tim.eckhardt@uni-hamburg.de)

Abstract. Arctic tundra ecosystems are currently facing rates of amplified climate change. This is critical as these ecosystems store significant amounts of carbon in their soils, which can be mineralized to CO_2 and CH_4 and released to the atmosphere. To understand how the CO_2 net ecosystem exchange (NEE) fluxes will react to changing climatic conditions, it is necessary to understand the individual responses of the physiological processes contributing to CO_2 NEE. Therefore, this study aimed: i) to partition NEE fluxes at the soil-plant-atmosphere interface in an arctic tundra ecosystem; and ii) to identify the main environmental drivers of these fluxes. Hereby, the NEE fluxes were partitioned into gross primary productivity (GPP) and ecosystem respiration (R_{eco}) and further into autotrophic (R_A) and heterotrophic respiration (R_H). The study examined flux data collected during the growing season in 2015 using closed chamber measurements in a polygonal tundra landscape in the Lena River Delta, northeastern Siberia. The measured fluxes on the microscale (1 m – 10 m) were used to model the NEE, GPP, R_{eco}, R_H, R_A and net ecosystem production (NPP) over the growing season. Here, for the first time, the differing response of *in situ* measured R_A and R_H fluxes from permafrost-affected soils to hydrological conditions have been examined. It was shown that low R_A fluxes are associated to a high water table, most likely due to the submersion of mosses, while an effect of water table fluctuations on R_H fluxes was not observed. Furthermore, this work found the polygonal tundra in the Lena River Delta to be a sink for atmospheric CO_2 during the growing season. Spatial heterogeneity was apparent with the net CO_2 uptake at a wet, depressed polygon center being more than twice as high as that measured at a drier polygon rim. In addition to higher GPP fluxes, the differences in NEE between the two microsites were caused by lower R_{eco} fluxes at the center compared to the rim. Here, the contrasting hydrological conditions caused the CO_2 flux differences between the microsites, where high water levels lad to lower decomposition rates due to anoxic conditions.

1 Introduction

More than 1,000 Petagrams of organic carbon (OC) are stored in the upper 3 m of northern permafrost-affected soils (Hugelius et al., 2014). Given the large amount of OC stored in these soils, the response of the arctic carbon (C) cycle to a changing climate is of global importance (McGuire et al., 2009). Over thousands of years, C has been sequestered in permafrost-affected soils and sediments due to cold conditions and poor drainage resulting in water saturation and slow organic matter decomposition. Currently, arctic ecosystems are facing amplified warming (Chapin et al., 2005), which will lead to the longer and deeper thawing of permafrost-affected soils

(Romanovsky et al., 2010). On the one hand, the microbial decomposition of liberated permafrost organic matter
40   releases carbon dioxide (CO_2) and methane (CH_4) (Grosse et al., 2011; Knoblauch et al., 2018; Knoblauch et al.,
2013; Schuur et al., 2009; Zimov et al., 2006a). On the other hand, higher temperatures increase the assimilation
of CO_2 by tundra vegetation due to a longer growing period and increased nutrient availability in the deeper layers
of thawed soils (Jia et al., 2009; Schuur et al., 2007).

Although the CO_2 budget of the arctic tundra has been the topic of several studies (e.g. Kittler et al., 2016; Kutzbach
45   et al., 2007b; Marushchak et al., 2013; Merbold et al., 2009; Oechel et al., 2000) the extent of their source or sink
strength has not been well established. Based on flux measurements, atmospheric inversion and process models,
McGuire et al. (2012) report that the arctic tundra still acts as a sink for atmospheric CO_2 on an annual basis with
a total CO_2 uptake of 110 Teragram (Tg) C yr^{-1}. However, this value is associated with a high uncertainty ranging
from 291 Tg C yr^{-1} uptake to 91 Tg C yr^{-1} loss. In contrast, in a meta-analysis of available flux observations in the
50   arctic tundra Belshe et al. (2013) report that these ecosystems act as source for atmospheric CO_2 (462 Tg C yr^{-1}).
However, the vast majority of the flux measurements taken into account by Belshe et al. (2013) have been
conducted in North America although the Russian arctic comprises an area of 3 million km^2 (CAVM-Team, 2003)
which is a large amount of the global tundra region. These current uncertainties in the arctic CO_2 budget clearly
show the need for intensified CO_2 flux observations in tundra ecosystems, in particular on the microsite scale (1-
55   10 m) in northern Siberia (Virkkala et al., 2017) as only a few studies are available from these ecosystems (e.g.
Corradi et al., 2005; Heikkinen et al., 2004; Kwon et al., 2016; Zamolodchikov et al., 2000). An improved
understanding of CO_2 dynamics in permafrost-affected soils is needed to improve estimates of future CO_2 balances
of the highly heterogeneous arctic tundra regions. Without furthering knowledge, estimates of the carbon balance
of the circum-arctic tundra and its future reaction to changing climatic conditions remain biased.

60   The net ecosystem exchange (NEE) of CO_2 between the land surface and the atmosphere is composed of the CO_2
uptake by plants, termed the gross primary productivity (GPP); and the release of CO_2 from soils and plants, the
ecosystem respiration (R_{eco}) (Chapin et al., 2006). The latter can further be split into autotrophic respiration by
plants (R_A) and heterotrophic respiration (R_H) mainly by microorganisms that decompose soil organic matter.
Inorganic sinks and sources of CO_2 are generally neglected because of their minor contribution to NEE (Elsgaard
65   et al., 2012; Kuzyakov, 2006). In order to partition NEE into the underlying fluxes, measurements of GPP, R_{eco},
R_A and R_H are required. These individual process-based fluxes governing the CO_2 balance react differently to
changing climatic conditions.

The release of CO_2 from soils by R_{eco} is the largest efflux of C from terrestrial ecosystems to the atmosphere
(Mahecha et al., 2010). R_A can be separated into aboveground plant respiration and belowground root respiration.
70   R_H is associated with the decomposition of soil organic matter (SOM) by heterotrophic soil organisms. It is
challenging to separate belowground respiration fluxes into autotrophic and heterotrophic components because
roots and microorganisms are closely linked within the rhizosphere (Hanson et al., 2000). There is a wide range
of methods to partition ecosystem respiration (Kuzyakov, 2006; Subke et al., 2006), each with its associated
advantages and disadvantages. Root trenching for example, despite some disturbance on the plant-soil interface,
75   can give accurate estimates of the rates of R_A and R_H (Diaz-Pines et al., 2010) and produces similar results as a
non-disturbing ^{14}C partitioning approach in an arctic tundra ecosystem (Biasi et al., 2014) and a partitioning
approach based on ^{13}C (Chemidlin Prévost-Bouré et al., 2008).

To date, a few estimates on the contribution of R_H to R_{eco} from tundra ecosystems during the growing season have
been published (Biasi et al., 2014; Nobrega and Grogan, 2008), with data lacking for ecosystems such as the

80 polygonal tundra. This is critical, as warming of the Arctic will influence R_{eco} fluxes both directly and indirectly:
Warming will increase decomposition of soil organic matter (R_H), but it will also cause permafrost to thaw, which
will expose previously frozen SOM to microbial decomposition (Dorrepaal et al., 2009; Schuur et al., 2011). This
could cause a substantial reduction of the carbon sink function of arctic tundra ecosystems as gross ecosystem
productivity has been found to be less temperature-sensitive than R_{eco} in these ecosystems (Dorrepaal et al., 2009;

85 Grogan and Chapin, 2000). Furthermore, warming could reduce microbial biomass (Frey et al., 2008) and soil
moisture (Suseela et al., 2012), and increase R_A due to increasing aboveground biomass, which can lead to a lower
contribution of R_H to R_{eco} (Chen et al., 2016; Hicks Pries et al., 2015). The increase of R_A and R_H fluxes due to
warming might be compensated by higher net primary production (Hicks Pries et al., 2013), but whether this is
valid for the complete growing season and across the highly heterogeneous arctic ecosystems remains uncertain.

90 The current study improves the understanding of CO_2 flux dynamics in permafrost-affected ecosystems of
northeastern Siberia by partitioning CO_2 NEE into its underlying processes: photosynthesis, ecosystem respiration
as well as autotrophic and heterotrophic respiration at two typical polygonal tundra microsites. Furthermore, the
response of these processes to different environmental parameters such as temperature and hydrology is revealed.
Finally, a CO_2 budget for a nearly complete vegetation period is determined for the two microsites using data-

95 calibrated flux models. These models were based on the time-sensitive bulk flux partitioning model by Runkle et
al. (2013), which was used in different arctic ecosystems (Helbig et al., 2017; Zona et al., 2014).

2 Study site

The investigation area is located on Samoylov Island in the southern central Lena River Delta, northeastern Siberia
(72°22'N, 126°28'E – Figure 1). The Lena river forms the largest delta in the Arctic, which can be

100 geomorphologically divided in river terraces of different ages and flood-plain levels (Schwamborn et al., 2002).
The delta is located in the continuous permafrost zone with permafrost extending to depths of down to 300 to
500 m (Yershov, 1998) and relatively low mean annual soil temperatures of -7.8 °C at 1.7 m depth (Boike et al.,
2013). With low temperatures and low precipitation, the study site has an arctic continental climate. The mean
annual air temperature between 1998 and 2011 was -12.5 °C, and mean annual rainfall is 125 mm, ranging from

105 52 mm to 199 mm (Boike et al., 2013). Polar day lasts from 7 May until 8 August, and polar night lasts from 15
November to 28 January. Snowmelt usually starts in the first half of June, and growing season usually occurs from
around mid-June until mid-September.

The study site is covered by an ice-wedge polygonal tundra on a Late-Holocene river terrace with elevations from
10 to 16 m above sea level on the eastern part of Samoylov Island. The development of polygonal structures has

110 created depressed polygon centers surrounded by elevated polygon rims with elevation differences of about 0.5 m.
Underlying permafrost prevents drainage in polygon centers with water-saturated soils, anoxic conditions at
shallow depths, and significant amounts of soil organic carbon of around 33 kg m^{-2} in the uppermost meter
(Zubrzycki et al., 2013). In contrast, the elevated polygon rim soils accumulated less soil organic carbon of around
19 kg m^{-2} (Zubrzycki et al., 2013) due to oxic conditions in the top soil. The land cover ratio of the polygonal

115 tundra on Samoylov Island is 65% for polygon rims, 19% for polygon centers and 16% for open water bodies
(Muster et al., 2012).

In this study, two different microsites were investigated: i) a wet-depressed polygon center; and ii) its surrounding
elevated polygon rim (72°22,442 N; 126°29.828 E). These microsites were located within the footprint area of an

eddy covariance (EC) system (Kutzbach et al., 2007b; Runkle et al., 2013; Wille et al., 2008). At this polygon, the

120 maximum active layer depth (ALD) was deeper at the polygon center (40 cm) compared to the polygon rim (30 cm). The soils at the polygon centers were classified as *Histic* or *Reductaquic Cryosols* with water table close to the soil surface (WRB, 2014). Polygon rim soils were characterized by cryoturbation and therefore classified as *Turbic Glacic Cryosols* with a water table just a few centimeters above the permafrost table. Total organic carbon (TOC) contents above 10% were found in the surface horizon (0-6 cm) above the cryoturbated horizons of the

125 polygon rim at the study site, while high TOC contents at the polygon center were found in the entire active layer. The vegetation of the polygon rims were dominated by mosses (*Hylocomium splendens, Polytrichum spp., Rhytidium rugosum*), some small vascular plants (*Dryas punctata* and *Astragalus frigidus*) as well as lichens (*Peltigera spp.*) and was classified after Walker et al. (2005) as non-tussock sedge, dwarf-shrub, moss tundra. The vegetation of the polygon centers were dominated by the hydrophilic sedge *Carex aquatilis* and mosses

130 (*Drepanocladus revolvens, Meesia triqueta, Scorpidium scorpioides*) and was classified as sedge, moss, dwarf-shrub wetland according to Walker et al. (2005).

3 Methods

3.1 Meteorological data

Meteorological variables were recorded at 30 minute intervals at the nearby EC system and adjacent

135 meteorological station 40 m southwest of the study site. Data on relative humidity and air temperature (MP103A, ROTRONIC AG, Switzerland), air pressure (RPT410F, Druck Messtechnik GmbH, Germany) and photosynthetically active radiation (PAR; wavelength: 400 – 700 nanometers; QS2, Delta-T Devices Ltd., UK) as well as the incoming and reflected components of shortwave and longwave radiation, respectively (CNR 1, Kipp and Zonen, Netherlands), were collected. The radiative surface temperature (T_{surf}; in Kelvin (K)) was calculated

140 as:

$$T_{surf} = \left(\frac{L\uparrow_B}{\varepsilon\,\sigma}\right)^{1/4} \tag{1}$$

where $L\uparrow_B$ is the upward infrared radiation (W m^{-2}), σ is the Stefan-Boltzmann constant (W m^{-2} K^{-4}), and the dimensionless emissivity ε was assumed to be 0.98 after Wilber et al. (1999). Furthermore, soil temperature was measured at 2 cm soil depth in intervals of 30 minutes at an adjacent polygon rim and center.

145   3.2 Soil sampling and vegetation indices

A total of six soil samples were taken from the thawed layer at the polygon rim using steel rings. At the polygon center, one soil sample was taken from the thawed layer using a spade, and separated into four soil layers based on their degradation status. Soil samples were homogenized for analysis of soil water content (mass difference between wet and dried (105 °C) soil samples), pH (CG820, Schott AG, Mainz, Germany) total C and nitrogen (N)

150 contents (VarioMAX cube, Elementar Analysesysteme GmbH, Hanau, Germany), as well as total organic carbon (TOC, liquiTOC II, Elementar Analysesysteme GmbH, Hanau, Germany) and total inorganic C (difference between total C and TOC). To analyze vegetation indices, gridded quadrats of 10 cm x 10 cm squares were placed over the collars, and a visual identification of the plant species present as well as their abundance (% surface cover) was conducted in four grid squares.

3.3 Net ecosystem exchange and ecosystem respiration

A total of eight PVC collars (50 cm x 50 cm), four at each microsite, were installed in July 2014 in preparation for NEE and R_{eco} flux measurements with closed chambers the following year. The collars were equipped with a U-shaped frame filled with water to avoid gas exchange between the chamber headspace and ambient air. The chamber (50 cm x 50 cm x 50 cm) used for NEE and R_{eco} flux measurements was made of clear plexiglas (Plexiglas SunActive GS, Evonik Industries AG, Germany). The chamber was equipped with a fan for continuous mixing of headspace air (axial fan, 12V/DC, Conrad Electronic SE, Germany). Furthermore, a PAR sensor (SKP212, Skye Instruments Ltd., UK) and a temperature probe (107 Thermistor probe, Campbell Scientific Ltd., USA) were installed inside the chamber. Including the volume inside the chamber collars, the chamber enclosed a volume of 124 - 143 L. For R_{eco} measurements, the chamber was covered with an opaque box (dark chamber measurements). Boardwalks were installed at both microsites to avoid disturbance. The volumetric soil water content (VWC) was measured with a GS3 sensor (Decagon Devices, Inc., USA) during each measurement directly beside the chamber collar in a depth of 5 cm. A diver (Schlumberger Ltd., USA) was installed at the polygon center to measure water table (WT) depth every 15 minutes. To prevent pressure-induced gas release during chamber closure (Christiansen et al., 2011), two holes (3 cm in diameter) at the top of the chamber were left open while placing the chamber on the collars and then closed for measurements. Soil temperatures between the surface and the frozen ground in 5 cm intervals and thaw depth were measured daily at both microsites. For each chamber flux measurement, CO_2 concentrations in the chamber headspace were continuously measured with an Ultra-Portable Gas Analyzer (UGGA 30-p, Los Gatos Research, USA). The chamber headspace was pumped in a closed loop system via transparent polyurethane tubes (inner diameter 4 mm, each 10 m length) through the analyzer with a flowrate of 200 mL min^{-1}. The CO_2 concentration was logged (CR800series, Campbell Scientific Ltd., USA) together with PAR as well as soil and air temperature at a frequency of 1 Hz. Each chamber measurement was restricted to 120 sec to minimize warming inside the chamber relative to the ambient environment.

Chamber measurements were conducted from 11 July until 22 September 2015. The chamber measurements were done at least every third day between 6 am and 9 pm (local time), apart from the period 2-9 August and 17-24 August. Two consecutive measurements were performed at each collar: first, NEE (n = 679) was measured with the transparent chamber, followed by an R_{eco} measurement (n = 679) with the dark chamber shortly after. The four collars of one microsite were measured in sequence before moving to the other microsite. GPP fluxes were calculated from the sum of the measured R_{eco} and NEE fluxes.

3.4 Heterotrophic respiration

For R_H measurements the root-trenching method was applied at both microsites. By inserting PVC collars 20 cm deep into the soil, which is below the main rooting zone, lateral roots were cut off. All living plant biomass including living moss tissue inside the collars were removed carefully in 2014. To prevent re-growth, the living plant biomass was removed periodically over the measurement period. This removal causes the die-off of roots, and days after the disturbance R_H equals NEE. A total of eight collars, four at each microsite, were prepared for R_H measurements. R_H fluxes (n = 662) were measured during the same periods and with the same measurement interval as NEE and R_{eco} measurements on unaltered plots.

To test if R_H fluxes are related to artefacts from the root-trenching approach, four additional PVC collars (two per microsite) were installed in 2015 following the sampling and preparation protocol of 2014. A total of 302 R_H flux

195   measurements were made on these newly installed plots. The differences of the mean R_H fluxes of each single plot
that was trenched in 2014 and 2015 were analyzed using a student's t-test.

R_A fluxes at the unaltered sites were calculated by subtracting the mean of the measured R_H fluxes from the four
replicate plots at the trenched sites from the mean of the measured R_{eco} fluxes at the unaltered sites from the same
day. The calculated R_A fluxes summed with GPP to estimate the net primary productivity (NPP) fluxes.

200   **3.5 Flux calculation**

CO_2 fluxes (µg CO_2 m^{-2} s^{-1}) were calculated using MATLAB® R2015a (The MathWorks Inc., Natick, MA, 2000)
with a routine that uses different regression models to describe the change in the chamber headspace CO_2
concentration over time and conducts statistical analysis to aid model selection (Eckhardt and Kutzbach, 2016;
Kutzbach et al., 2007a).

205   Due to possible perturbations while placing the chamber on the collar, the first 30 seconds of each 2-minute
measurement period were discarded and the remaining 90 data points were used for flux calculations. The precision
of the gas analyzer with 1 s signal filtering is < 0.3 ppm for CO_2. Typically, the root mean square error (RMSE)
of chamber measurements and the fitting of the linear and non-linear regression models did not exceed this value,
and higher RMSE values indicated failed model fitting or disturbed chamber measurements. Therefore, if RMSE

210   exceeded 0.3 ppm, the concentration-over-time curve was re-inspected. Variation of PAR during chamber
measurements due to shifts in cloud cover leads to irregular CO_2 concentration time series and perturbation of the
calculated CO_2 fluxes (Schneider et al., 2011). These perturbed concentration time series show distinct
autocorrelation of the residuals of the regression models and were filtered out by using a threshold for residual
autocorrelation indicated by the Durbin-Watson test (Durbin and Watson, 1950). If the RMSE exceeded 0.3 ppm

215   or showed a distinct autocorrelation, the flux curve was re-inspected to see if irregularities could be removed by
adjusting the time series. If irregularities could be removed by adjusting the time series, the flux curve was
re-calculated and if not, the dataset was discarded. Overall, about 3% (n = 47) of the CO_2 flux measurements (NEE,
R_{eco} and R_H measurements) were discarded from the dataset, because they did not meet the abovementioned quality
criteria.

220   It was shown that CO_2 fluxes calculated with linear regression models can be seriously biased (Kutzbach et al.,
2007a), while non-linear regression models significantly improve flux calculations (Pihlatie et al., 2013). However,
we found that the change in CO_2 concentration in the chamber was modelled best with a linear regression model,
as determined by the *Akaike* Information Criterion corrected for small samples sizes (AIC$_c$) (Burnham and
Anderson, 2004). This is in good agreement with other studies, which have shown that in some cases a linear

225   regression model can produce a better CO_2 flux estimate for a non-linear concentration-over-time curve than a
non-linear regression model (Görres et al., 2014; Koskinen et al., 2014).

3.6 Modelling CO_2 fluxes

In this study the atmospheric sign convention is used, whereby a positive NEE defines a net release of CO_2 from
the soil to the atmosphere. To determine their single contribution to the NEE, different a range of numerical models

230   were fitted to the measured CO_2 fluxes to quantify seasonal GPP, R_{eco}, and R_H fluxes.

To calibrate the models, the used functions were fitted to the GPP, R_{eco}, and R_H fluxes. The resulting fitting
parameters were used to reproduce the fluxes over the complete measurement period. Model calibration was done
by applying a 15-day moving window over the measurement period moving on a daily basis. If less than eight

chamber measurements were performed during these 15 days, the moving window was extended to 19 days.

235   Subsequently, the modelled fluxes for each measurement plot were averaged for each microsite. CO_2 fluxes from each of the four measurement plots were used separately for model calibration and the summed fluxes were used to analyze differences between both microsites using a student's t-test.

The empirical Q_{10} model (van't Hoff, 1898) was fitted to the measured R_{eco} and R_H fluxes:

$$R_{eco,H} = R_{base} \times Q_{10}^{\frac{T_{a,surf,soil} - T_{ref}}{\gamma}} \tag{2}$$

240   where the fit parameter R_{base} was the respiration at the reference temperature T_{ref} (15 °C). T_{ref} and γ (10 °C) were held constant according to Mahecha et al. (2010). Q_{10} was a fit parameter indicating the ecosystem sensitivity of respiration to a 10 °C change in temperature. For this study a fixed Q_{10} value of 1.52 was used, which represents the seasonal mean value of the bulk partitioning model for the CO_2 fluxes in the EC footprint area established by Runkle et al. (2013). Air temperature (T_a), surface temperature (T_{surf}), and soil temperature (T_{soil}) measured at a

245   depth of 5 cm were tested as input variables.

The model calibration was done with MATLAB® R2015a (The MathWorks Inc., Natick, MA, 2000). The model parameters were estimated by nonlinear least-squares regression fitting (nlinfit function), and the uncertainty of the parameters was determined by calculating the 95% confidence intervals using the nlparci function. The selection of the best performing temperature as input variable for the R_{eco} and R_H model was based on comparing

250   the R^2_{adj} of the model runs with different temperatures as input variable. The selected input variable was chosen for all measurement plots of the same microsite, although at times for a given plot a different input variable might have had a better R^2_{adj}.

To estimate GPP, the chamber measured R_{eco} fluxes were subtracted from the NEE fluxes separately for each measurement plot. The rectangular hyperbola function was fitted to the calculated GPP fluxes as a function of

255   PAR (in µmol m^{-2} s^{-1}):

$$GPP = -\frac{P_{max} \times \alpha \times PAR}{P_{max} + \alpha \times PAR} \tag{3}$$

where the fit parameter P_{max} was the maximum canopy photosynthetic potential (hypothetical maximum of P_{max} at infinite PAR). The values for the initial canopy quantum efficiency α (dimensionless; initial slope of the P_{max} -PAR curve at PAR = 0) were obtained from modelling the CO_2 fluxes with EC data (Kutzbach et al., unpublished).

260   From the determined values when α was held variable, a function was formulated that account for the seasonality of α with specific values for every day of the growing season using the following function:

$$\alpha = b \times exp^{\left(-\frac{abs\left((x-c)^d\right)}{2 \times e^2}\right)} + f \tag{4}$$

where $b = 0.042$, $c = 209.5$, $d = 2$, $e = 25.51$, $f = 0.008$ and $x =$ day of year 2015. Afterwards, these values (variable on daily basis) were used to reproduce GPP fluxes from chamber measurements over the complete

265   measurement period.

Although the transmissivity of the chamber material was high (> 92%), it caused a reduction in the amount of incoming radiation reaching the surface. During the complete measurement period, the PAR values measured inside the chamber were on average 20% lower than the PAR values measured outside the chamber (data not shown). Therefore, GPP modelling was conducted in two steps. First, the GPP model was calibrated using PAR

270   values measured inside the chamber; and secondly, the reproduction of GPP fluxes over the growing season was carried out using PAR values measured outside the chamber. Without this two-step calibration the CO_2 uptake rates would have been underestimated.

The NEE fluxes were calculated as the sum of the modelled GPP and R_{eco} fluxes. The R_A fluxes were calculated as the difference of the modelled R_{eco} and R_H fluxes. Furthermore, NPP was calculated from the sum of R_A and GPP fluxes.

4 Results

4.1 Meteorological data and environmental conditions

From mid-July to the end of September 2015, soil temperatures at 2 cm depth at the polygon rim showed a higher diurnal variability than at the center. The highest soil temperatures were measured in mid-July and at the beginning of August. At the end of September, the temperatures became slightly negative (Figure 2). The mean daily air temperature ranged between 23 °C and -2 °C. Three warm periods were recorded, one in mid-July (up to 27 °C) and one at the beginning of August (up to 25 °C) and a third warm period was recorded at the beginning of September with temperatures of up to 20 °C. The average temperature in August 2015 (9 °C) was similar to the long-term mean temperature over the period 1998-2011 (Boike et al., 2013). Compared to the long-term mean, it was about 1°C colder during July (9 °C), whereas September was around 2 °C warmer than the reference period (3 °C). The total precipitation from mid-July to end of September 2015 was 78 mm.

At the polygon rim, the thaw depth increased from the beginning of the campaign in mid-July until mid-September to reach a maximum depth of 36 cm. Maximum thaw depth was reached at the polygon center much earlier in the season (mid-July) and remained relatively constant until mid-September. From mid-September onwards the thaw depth decreased slightly until the end of September at both microsites. The water table depth at the polygon center were tightly coupled to rainfall. The VWC at 5 cm soil depth was on average 30% at the polygon rim, with highest values observed after rainfall events (Figure 2).

Photosynthetically active radiation showed strong diurnal variability, with lowest PAR values during nighttime. From mid-July until 12 August, mean nighttime (9 pm – 3 am) PAR values did not drop below 5 µmol m^{-2} s^{-1} (Figure 2). Afterwards, with upcoming polar night conditions, the number of periods with PAR values below 5 µmol m^{-2} s^{-1} increased. Midday PAR values above 1000 µmol m^{-2} s^{-1} were measured in mid-July, at the beginning of August, and once at the end of August. Throughout September, the daily maximum PAR values were decreasing.

The total soil C content was lower at the polygon rim (2-12%) than the polygon center (10-20%) and showed a reduction with depth. At the polygon center the N content showed little variability with depth, with being around 0.6%, and the C/N ratio decreased from 33.1 at the surface to 16.9 at the bottom of the active layer. In contrast, in the polygon rim, the N content was considerably higher in the organic-rich layer compared to the mineral soil layer (0.5% vs. 0.1%), and the difference of the C/N ratio at different soil depths was smaller than in the center. Strongly acidic pH values were measured throughout the active layer of both microsites, with values around 5.3 at the polygon center, while in the organic-rich layer and in the mineral soil layer at the rim the pH was moderately acidic with values of 5.7 and 6.0, respectively.

4.2 Carbon dioxide fluxes

The highest NEE fluxes were measured at the end of July with -97 ± 27 µg CO_2 m^{-2} s^{-1} and -209 ± 17 µg CO_2 m^{-2} s^{-1} at the rim and center (Figure 3), respectively. In September, both microsites acted as small net sources of atmospheric CO_2. The net CO_2 uptake at the center was generally higher than at the rim. The

highest net CO_2 release at the polygon rim was measured on 17 August with 16 ± 5 µg CO_2 m^{-2} s^{-1}, and at the polygon center on 19 September with 22 ± 3 µg CO_2 m^{-2} s^{-1}. The standard error of the flux calculation was about 3.5 and 2.3 µg CO_2 m^{-2} s^{-1} for polygon center and rim, respectively, and decreased slightly towards the end of the season.

315   In contrast to the NEE fluxes, the measured R_{eco} fluxes were on average higher at the rim compared to the center. The lowest ecosystem respiration fluxes at the polygon center were observed on 23 July with 10 ± 3 µg CO_2 m^{-2} s^{-1} and at the polygon rim on 21 September with 17 ± 1 µg CO_2 m^{-2} s^{-1}. The highest ecosystem respiration fluxes of 80 ± 11 and 88 ± 10 µg CO_2 m^{-2} s^{-1} for rim and center, respectively, were measured at 9 August, when the air temperature exceeded 20 °C.

320   The net CO_2 uptake increased from mid-July until it peaked during the vegetation maximum at the end of July and beginning of August. Subsequently, NEE decreased until the end of September. This seasonality was more pronounced at the polygon center than at the polygon rim. Interestingly, towards September the net CO_2 uptake at the polygon rim exhibited an increase for a period of about one week until it decreased again towards the end of September. R_{eco} fluxes showed a similar, but less distinct seasonal pattern, and the peak of the highest R_{eco} fluxes

325   was in mid-August. In contrast, R_H fluxes showed no seasonal trend.

The lowest GPP fluxes were calculated for the end of September with -10 ± 3 µg CO_2 m^{-2} s^{-1} and -16 ± 6 µg CO_2 m^{-2} s^{-1} for the polygon center and rim, respectively (Figure 3). The highest GPP fluxes at the polygon rim were found at the end of July and beginning of August with -143 ± 33 µg CO_2 m^{-2} s^{-1} as well as at the polygon center with -245 ± 19 µg CO_2 m^{-2} s^{-1}.

330   The calculated R_A fluxes at the polygon center were on average 18 ± 14 µg CO_2 m^{-2} s^{-1} with highest fluxes of 56 ± 10 µg CO_2 m^{-2} s^{-1} measured on 17 August. At the polygon rim, the averaged calculated R_A flux was 16 ± 8 µg CO_2 m^{-2} s^{-1}. At this microsite, the highest R_A flux of 42 ± 7 µg CO_2 m^{-2} s^{-1} was observed on 18 July, and the lowest R_A flux was observed at mid-September with 3 ± 9 µg CO_2 m^{-2} s^{-1}.

As observed for the GPP fluxes, calculated NPP fluxes showed a distinct seasonality (Figure 3). The mean NPP

335   fluxes were -94 ± 61 and -55 ± 26 µg CO_2 m^{-2} s^{-1} at the polygon center and rim, respectively. The highest NPP flux at the center was on 30 July with -222 ± 18 µg CO_2 m^{-2} s^{-1}, which is three days earlier than the maximum GPP flux was determined. Similar to the highest GPP fluxes, the highest NPP flux at the rim was determined on 27 July with -115 ± 29 µg CO_2 m^{-2} s^{-1}. The lowest NPP fluxes were determined in September with -10 ± 11 µg CO_2 m^{-2} s^{-1} at the rim and -2 ± 6 µg CO_2 m^{-2} s^{-1} at the center.

340   The highest releases of CO_2 by R_H were measured on 9 August at the polygon center and rim with 38 ± 6 and 51 ± 12 µg CO_2 m^{-2} s^{-1}, respectively. The lowest R_H fluxes of 3 ± 1 µg CO_2 m^{-2} s^{-1} were measured at the center on 3 September, while at the rim lowest R_H fluxes of 10 ± 3 µg CO_2 m^{-2} s^{-1} were observed at the end of September. Increased R_H fluxes after periodical re-clipping of the vegetation were not observed. The comparison of R_H fluxes from measurement plots that were trenched in 2014 with those that were trenched in 2015 revealed no significant

345   differences (t-test, $p > 0.05$) between the years of root-trenching (data not shown).

Interestingly, the R_{eco} fluxes were linearly correlated with WT fluctuations from the beginning of July until the end of August (Figure 4). In contrast to this, neither a trend of higher R_H fluxes during times of high WT, nor lower R_H fluxes during times of low WT were observed. Instead, the R_A fluxes showed a good correlation ($R^2 = 0.71$; $p < 0.05$) with WT fluctuations.

4.3 Modelled CO₂ fluxes

The fitting parameter of the GPP model, P_{max}, showed strong spatial and temporal variability (Figure 5). The α values used for the GPP model showed a high temporal variability with a mean of 1.47 ± 0.62. This value increased sharply towards the peak vegetation period at the end of July and decreased afterwards towards the end of the growing season. The P_{max} values showed a strong temporal variability at the polygon center (mean: 250.7 ± 101.9 µg CO_2 m^{-2} s^{-1}). Considerable differences in P_{max} were also observed between polygon rim and center. The averaged P_{max} at the polygon rim (135.4 ± 37.2 µg CO_2 m^{-2} s^{-1}) was substantially lower than at the polygon center (250.7 ± 101.9 µg CO_2 m^{-2} s^{-1}). As with the measured NEE fluxes, P_{max} values displayed an increase at the polygon rim towards the end of September. The fitting parameter of the R_{eco} and R_H model, R_{base}, also showed a strong spatial and temporal variability (Figure 5). In general, R_{base} was higher at the polygon rim. The averaged R_{base} values for the R_H model fit differed substantially between microsites with 14.6 ± 2.1 µg CO_2 m^{-2} s^{-1} at the polygon center and 29.0 ± 2.9 µg µg CO_2 m^{-2} s^{-1} at the polygon rim.

The best model fit of polygon center R_{eco} fluxes ($R^2_{adj} = 0.70$) was achieved when the surface temperature was used as explanatory variable; while for the polygon rim the soil temperature showed the best fitting ($R^2_{adj} = 0.46$). In contrast to the R_{eco} fluxes, the best model fit for polygon center R_H fluxes was achieved when the air temperature was used as explanatory variable ($R^2_{adj} = 0.55$). At the polygon rim, using the soil temperature as explanatory variable showed the best fitting ($R^2_{adj} = 0.45$) when modelling R_H fluxes. However, differences in the goodness of the fits were small.

At the polygon rim, the averaged modelled R_{eco} fluxes were higher than at the center (Table 1), however the difference between the microsites was not statistically significant (t-test, $p > 0.05$). The highest R_{eco} values were encountered at both microsites at the beginning of August (Figure 6 and Figure 7). At the polygon rim, the lowest R_{eco} fluxes where obtained at the end of September, while the lowest fluxes at the polygon center where observed on 21 July, associated with the highest water table during the campaign.

At the polygon center, the modelled R_H fluxes were substantially lower than at the polygon rim, and this difference between the microsites was highly significant (t-test, $p < 0.001$). The lowest R_H fluxes at the center were encountered on 3 September, a period of low air temperatures. The highest R_H flux was observed when temperatures first rose above 25 °C in July. The highest and lowest modelled R_H fluxes at the polygon rim were encountered at the same time as the highest and lowest modelled R_{eco} fluxes (8 August and 20 September). When comparing modelled data for R_H and the R_{eco} over the whole measurement period, the contribution of R_H to R_{eco} was on average 42 % at the center and 60 % at the rim.

The modelled GPP fluxes showed a distinct seasonal trend. From the mid of July until 12 August, photosynthesis took place for 24 hours per day because of polar day conditions, even though the CO_2 uptake was low during nighttime. Afterwards, periods when GPP was zero extended due to extended night conditions. At both microsites, the diurnal amplitude of GPP increased from the beginning of the campaign until it reached a maximum in mid-August. After this peak, the GPP fluxes at the center continuously decreased until the lowest daily maximum GPP on 21 September at the polygon center. Interestingly, the lowest daily GPP maximum at the polygon rim was observed about a week earlier than at the polygon center. Later, the GPP at the polygon rim increased again. The difference in GPP fluxes between the microsites was statistically significant ($p < 0.01$). The R^2_{adj} of the GPP model was 0.82 for the polygon center and 0.45 for the polygon rim.

The modelled GPP and R_{eco} fluxes were used to calculate NEE fluxes. The highest net CO_2 uptake at the rim was encountered on 23 July and on 16 August at the polygon center, while the highest net CO_2 release was measured

at both microsites on 17 August. The diurnal amplitude of NEE oscillation was greatest between the end of July and mid-August. The modelled R_{eco} and R_H fluxes were used to calculate R_A fluxes. Therefore, the lowest and highest R_A fluxes were similar to the R_{eco} and R_H fluxes. The modelled R_A fluxes correlated substantially with WT fluctuations with lowest R_A fluxes during times of lowest WT. The NPP fluxes were calculated from the sum of

395 GPP and R_A fluxes. At both microsites the highest NPP was encountered in mid-August, while the lowest daily net primary productivity was in mid-September. At the polygon center the NPP showed a distinct seasonal trend, while at the polygon rim this trend less clear.

4.4 Integrated fluxes

Based on the modelled CO_2 fluxes, the time-integrated CO_2 fluxes for the period between mid-July and end of

400 September 2015 were calculated (Figure 8). The integrated net CO_2 uptake (NEE) was more than twice as high at the center than at the rim. The integrated GPP flux at the polygon center was substantially higher than at the polygon rim. Interestingly, the integrated R_{eco} flux at the rim was higher than at the center, and an almost twice as high R_H flux at the rim was observed. The integrated R_A fluxes at polygon center and rim were within the same range. During the vegetation period, the NPP was almost twice as high at the center compared to the rim.

405 ## 5 Discussion

This study presented the first values of NEE, GPP, NPP as well as R_{eco}, R_H and R_A fluxes obtained from modelling approaches for different microsites of the polygonal tundra were presented. These fluxes are of crucial importance as they show the different response that the underlying processes governing CO_2 NEE have to environmental controls over the growing season, both spatially and temporally. Both the water-saturated polygon center and the

410 non-saturated polygon rim acted as net sinks for atmospheric CO_2 for the period from mid-July to end of September 2015. The CO_2 sink strength differed substantially between the microsites, which is related to the different hydrological conditions. The integrated R_{eco} fluxes at the rim were higher than at the center. This is remarkable as R_{eco} fluxes are expected to rise with increasing GPP fluxes (Bubier et al., 2003), since CO_2 uptake via photosynthesis is the source of R_A fluxes. However, despite substantial higher GPP fluxes, the R_A fluxes at the

415 center were within the same range as those at the rim. Furthermore, higher R_{eco} fluxes at the polygon rim compared to the center were also caused by the higher rim R_H fluxes due to drier soil conditions. Overall, the differences in R_A and GPP fluxes between the two microsites led to NPP at the polygonal center being almost two-times higher than at the polygon rim.

5.1 CO_2 fluxes from arctic tundra sites

420 The modelled R_{eco} fluxes at both studied microsites were at the lower end of those reported for other arctic tundra sites with similar vegetation and soil composition (Table 2). Solely, a wet tundra site in the Komi Republic, Russia (Heikkinen et al., 2004), a wet sedge site at Daring Lake, Canada (Nobrega and Grogan, 2008) and a polygon center site in Alaska (Oechel et al., 1995) showed R_{eco} fluxes that were within the same range as in this study. The comparison of partitioned CO_2 fluxes from different arctic tundra sites highlighted the importance of individual

425 GPP and R_{eco} fluxes to explain NEE fluxes. The comparatively low R_{eco} fluxes and moderate GPP fluxes reported from this study led to relatively high NEE fluxes at the polygon center, compared to other tundra sites. Furthermore, the highest net CO_2 uptake fluxes were reported from wet and sedge-dominated sites. The GPP fluxes

at the two studied microsites are lower than reported fluxes from most arctic study sites (Olivas et al., 2011; Ström et al., 2012; Vourlitis et al., 2000; Zamolodchikov et al., 2000).

430 **5.2 Environmental controls on CO₂ fluxes**

The polygonal tundra on Samoylov Island had to be considered as an ecosystem with low GPP due to low vascular plant coverage with a maximum leaf coverage of 0.3 (Kutzbach et al., 2007b). Mosses, which have a high leaf coverage (> 0.9), were dominant at both microsites and have, similar to lichens, a much lower photosynthetic capacity than vascular plants (Brown et al., 1980). Furthermore, photosynthesis of vascular plants is restricted in
435 arctic tundra ecosystems due to the low nutrient availability. Low nutrient availability is typical for most tundra soils due to water saturation and low soil temperatures (Oechel et al., 1998), as these conditions ensure low microbial decomposition rates (Hobbie et al., 2002), which in turn result in a low supply of bioavailable nutrients (Beermann et al., 2015). Nitrogen stocks at the studied microsites were rather low compared to other arctic tundra sites (Harden et al., 2012). Additionally, the net radiation at the study site from June to August was with a mean
440 of 85 W m⁻² (1999-2011) lower than those reported from most other arctic tundra sites (cf. Boike et al., 2013; Lynch et al., 1999; Soegaard et al., 2001). These factors might explain the comparatively low GPP fluxes at the polygon rim and center compared to other arctic tundra sites.

Differences in GPP between the rim and center can be related to the vascular plant coverage. The polygon center had a much higher abundance of sedges, while the rim was moss-dominated and the sparsely spread vascular plants
445 had shorter and fewer leaves. Therefore, the photosynthetic capacity of the center is higher than the rim, resulting in higher GPP. Additionally, limited water availability due to the elevation of the polygon rim caused moisture to run off, with a drier or desiccated moss layer potentially contributing to lower GPP (Olivas et al., 2011). On the other hand, Olivas et al. (2011) found GPP fluxes to be higher at a polygon rim than at a polygon center in the Alaskan coastal plains. They related low GPP fluxes at the center to submersion of the moss layer and vascular
450 plants. At the polygon center of the current study, the WT was frequently below the soil surface so that submersion of erect vascular plants was not observed regularly, and even the moss layer was not submerged for most of the time. This difference in GPP between the Alaskan study sites (Olivas et al., 2011) and those presented in this study reveals the importance of water level and its fluctuations throughout the season.

Differences in NEE fluxes between the two microsites can also be related to their different soil conditions. The
455 cold and water-logged conditions typical of the polygon centers, inhibited decomposition and mineralization of SOM due to oxygen limitation, which caused low microbial activity (Hobbie et al., 2002; Walz et al., 2017). Furthermore, the moisture run-off at the rim created drier conditions in the top soils at the rim, which increased soil oxygen availability and therefore enhanced R_H and R_{eco} (Oechel et al., 1998). The higher diurnal amplitude of the soil temperature, a product of the thermic buffer function of the standing water at the center, led to higher daily
460 soil temperatures at the polygon rim compared to the center. Both the higher temperatures and oxygen supply enhanced microbial decomposition and therefore higher R_H fluxes at the polygon rim compared to the polygon center. Hence, low net carbon uptake at the rim occurred not only because of low GPP, but also due to higher R_H fluxes compared to the center. This finding is in good agreement with Nobrega and Grogan (2008) who compared a wet sedge with a dry heath and a mesic birch site and found that the net carbon uptake at the wet sedge site was
465 highest because of limited respiration due to water-logged conditions.

Interestingly, measurements of CO₂ fluxes at the polygon rim showed an increase of NEE throughout September, whereas at the polygon center the net CO₂ uptake appeared to continuously decrease. This increase at the rim

cannot be explained by rising PAR or temperature. Rather, the increase of net CO_2 uptake at the rim towards the end of September may be related to the photosynthetic activity of mosses. Kutzbach et al. (2007b) considered the

470   September at the EC footprint area as period where C uptake occurs mostly due to moss photosynthesis. During this time of the growing season, mosses can still assimilate substantial amounts of CO_2 because they tend to reach light saturation at lower irradiance (Harley et al., 1989). The photosynthetic activity of mosses declines rapidly when they face desiccation, because they cannot control their tissue water content (Turetsky et al., 2012). It was also shown that mosses face light stress during times of high PAR (Murray et al., 1993). This light stress causes

475   delayed senescence and more late-season photosynthesis (Zona et al., 2011). Therefore, the photosynthetic activity at the polygon rim is expected to be low during warm and dry periods such as those seen at the beginning of September 2015, and during times of high PAR. With continuous rainfall, dew formation and lower PAR in mid-September, the mosses are likely resume metabolic active, which led to increasing net CO_2 uptake at the rim.

5.3 Partitioning respiration fluxes in arctic tundra ecosystems

480   To date only a handful of studies have estimated growing season R_H fluxes from arctic tundra ecosystems (Biasi et al., 2014; Nobrega and Grogan, 2008). Surprisingly, the differences between these estimates of R_H fluxes were rather low. Differences in R_H fluxes measured with the trenching method may be caused by differences in the time between trenching and start of the measurement. Nobrega and Grogan (2008) started the R_H measurements one day after clipping, while measurements in this study as well as in the study of Biasi et al. (2014) started about one

485   year after treatment. Therefore, even though the partitioning approach for seasonal estimates of R_H fluxes was similar for all studies, any comparison must be made with caution. The few R_H flux estimates reported from other arctic tundra sites were higher than the R_H values from the Lena River Delta (0.5 ± 0.1 and 0.3 ± 0.02 g C m^{-2} d^{-1} at polygon rim and center, respectively). Higher R_H fluxes throughout the growing season (0.8-1.8 g C m^{-2} d^{-1}) were measured at a mesic birch and a dry heath site at Daring Lake in Canada (Nobrega and Grogan, 2008) and at

490   a bare peat site (1.0 g C m^{-2} d^{-1}) in the subarctic tundra at Seida, Russia (Biasi et al., 2014). Both sites contained substantially higher amounts of SOC in the organic-rich layer than the soil at the polygon rim and were well-aerated compared to the soil at the polygon center, which both most likely caused a higher organic matter decomposition rate and could explain the higher R_H fluxes than at the polygonal tundra microsites. Similar R_H fluxes to those reported in our study were measured at a wet sedge site in Daring Lake (0.4 g C m^{-2} d^{-1}) (Nobrega

495   and Grogan, 2008), where soil and environmental conditions like WT, ALD, soil temperature, vegetation and SOC were similar to the Samoylov sites and at vegetated peat sites in Seida (0.4-0.6 g C m^{-2} d^{-1}) (Biasi et al., 2014). Despite these differences, the averaged contributions of R_H to R_{eco} of 42% at the center and 60% at the rim are in good agreement with those observed at Seida (37 – 64%) and Daring Lake (44 – 64%). Similar contributions were determined from an arctic tussock tundra site, where R_H makes up approximately 40% of growing season R_{eco}

500   (Segal and Sullivan, 2014) and from a moist acidic tussock tundra site (Hicks Pries et al., 2013). In contrast to these results, Dorrepaal et al. (2009) determined a substantially higher contribution of R_H to R_{eco} with about 70% in a subarctic peatland.

The difference in the contribution of R_H to R_{eco} between the polygon rim and center at our study site can be related to differences in vascular plant coverage and moisture conditions between both microsites. Higher GPP at the

505   center than at the rim caused also higher rates of R_A and in turn lowered the contribution of R_H to R_{eco}. Additionally, anoxic soil conditions due to standing water, like at the polygon center, were not favorable for decomposition of

SOM. Furthermore, Nobrega and Grogan (2008) concluded that consistently moderate moisture conditions, as at the polygon rim, promotes fast decomposition of SOM and therefore ensures higher R_H rates than at the center. Interestingly, at the polygon center, we observed significant correlations of the WT with R_{eco} and R_A fluxes, but

510 no correlation between R_H fluxes and WT. The R_A fluxes might be negatively affected by high WT due to submersion of the moss layer and partwise vascular leaf area as submersion can lead to plant stress, reducing productivity and nutrient turnover (Gebauer et al., 1995). Low soil moisture contents can limit the growth and productivity of an ecosystem (Chen et al., 2015) as desiccation lowers the photosynthetic activity (Turetsky et al., 2012), and in turn lowers R_A fluxes. However, if this were the case, we would expect a correlation between GPP

515 and WT, which was not observed. Instead, it is likely that the respired CO_2 is 'recycled' due to of slow diffusion through the moss layer. Evidence for this process was already shown in polygonal ponds (Liebner et al., 2011). This finding is in contrast to a set of studies who explained correlations between R_{eco} fluxes and WT fluctuations with the impact of oxygen availability on R_H fluxes (Chimner and Cooper, 2003; Dorrepaal et al., 2009; Juszczak et al., 2013) or observed an impact of moisture conditions on R_H fluxes across multiple peatland ecosystems

520 (Estop-Aragonés et al., 2018), while another study has shown no effect between water table fluctuations and R_{eco} fluxes (Chivers et al., 2009). However, these findings show the importance of the soil water content for R_{eco} fluxes and the need for partitioning approaches to understand the response of the underlying processes of R_{eco} fluxes on changing hydrologic conditions.

In order to determine the individual impacts of hydrological conditions and temperature on the R_H and R_A fluxes,

525 it would be useful to perform both warming and wetting experiments *in situ*. So far, a number of studies have determined the temperature response of NEE, GPP, and R_{eco} fluxes in arctic ecosystems with warming experiments (e.g. Frey et al., 2008; Natali et al., 2011; Voigt et al., 2016), however, much less research has focused on the response of R_A and R_H fluxes to increased temperatures (Hicks Pries et al., 2015). Wetting experiments in arctic tundra ecosystems to determine the individual response of R_A and R_H fluxes to changing hydrological conditions

530 are lacking so far, despite their importance as highlighted in this study, which is critical as climate warming will likely lead to severe changes of the hydrological regimes in Siberian tundra regions (Merbold et al., 2009; Zimov et al., 2006b).

6 Conclusion

The contributions of GPP, R_{eco}, R_H and R_A to CO_2 NEE fluxes in a drained (rim) and water-saturated (center)

535 microsite in the arctic polygonal tundra of northeast Siberia have been quantified in this study. Both investigated microsites acted as CO_2 sinks during the measurement period mid-July to end of September 2015. The polygon center acted as a considerably stronger CO_2 sink than the polygon rim. The main drivers behind these differences in CO_2 fluxes at the microsites were the higher GPP at the polygon center low R_H and R_A fluxes. The substantial differences identified in NEE between the two investigated microsites highlight the importance of microscale

540 measurements for reliable estimates of CO_2 surface-atmosphere fluxes from arctic tundra sites and the important role of soil moisture conditions on CO_2 fluxes. Hereby, it was shown that R_A and R_H fluxes respond differently depending on hydrological conditions, with low R_A fluxes during times of high water tables. Therefore, it is recommended that future studies determining partitioned CO_2 fluxes from arctic tundra ecosystems should focus on the role of hydrological conditions as a driver of these fluxes to obtain a more in-depth insight into this

545 relationship.

Biogeosciences
Discussions

Author contributions

TE, EMP and CK designed the study. GS and TE performed the chamber measurements and laboratory analysis. TE wrote the manuscript with contributions from all authors.

References

560   Beermann, F., Teltewskoi, A., Fiencke, C., Pfeiffer, E. M., and Kutzbach, L.: Stoichiometric analysis of nutrient availability (N, P, K) within soils of polygonal tundra, Biogeochemistry, 122, 211-227, 2015.

Belshe, E. F., Schuur, E. A., and Bolker, B. M.: Tundra ecosystems observed to be CO2 sources due to differential amplification of the carbon cycle, Ecology Letters, 16, 1307-1315, 2013.

Biasi, C., Jokinen, S., Marushchak, M. E., Hämäläinen, K., Trubnikova, T., Oinonen, M., and Martikainen, P. J.:

565   Microbial Respiration in Arctic Upland and Peat Soils as a Source of Atmospheric Carbon Dioxide, Ecosystems, 17, 112-126, 2014.

Boike, J., Grüber, M., Langer, M., Piel, K., and Scheritz, M.: Orthomosaic of Samoylov Island, Lena Delta, Siberia. PANGAEA, 2012.

Boike, J., Kattenstroth, B., Abramova, K., Bornemann, N., Chetverova, A., Fedorova, I., Fröb, K., Grigoriev, M.,

570   Grüber, M., Kutzbach, L., Langer, M., Minke, M., Muster, S., Piel, K., Pfeiffer, E. M., Stoof, G., Westermann, S., Wischnewski, K., Wille, C., and Hubberten, H. W.: Baseline characteristics of climate, permafrost and land cover from a new permafrost observatory in the Lena River Delta, Siberia (1998-2011), Biogeosciences, 10, 2105-2128, 2013.

Boike, J., Veh, G., Viitanen, L.-K., Bornemann, N., Stoof, G., and Muster, S.: Visible and near-infrared

575   orthomosaic of Samoylov Island, Siberia, summer 2015 (5.3 GB). PANGAEA, 2015.

Brown, J., Miller, P. C., Tieszen, L. L., and Bunnell, F.: An arctic ecosystem: the coastal tundra at Barrow, Alaska, Dowden, Hutchinson & Ross, Inc., Stroudsberg, PA, USA, 1980.

Bubier, J., Crill, P., Mosedale, A., Frolking, S., and Linder, E.: Peatland responses to varying interannual moisture conditions as measured by automatic CO2 chambers, Global Biogeochemical Cycles, 17, 1066, 2003.

580   Burnham, K. P. and Anderson, D. R.: Multimodel inference - understanding AIC and BIC in model selection, Sociological Methods & Research, 33, 261-304, 2004.

Chapin, F. S., Sturm, M., Serreze, M. C., McFadden, J. P., Key, J. R., Lloyd, A. H., McGuire, A. D., Rupp, T. S., Lynch, A. H., Schimel, J. P., Beringer, J., Chapman, W. L., Epstein, H. E., Euskirchen, E. S., Hinzman, L. D., Jia, G., Ping, C. L., Tape, K. D., Thompson, C. D. C., Walker, D. A., and Welker, J. M.: Role of

585   land-surface changes in Arctic summer warming, Science, 310, 657-660, 2005.

Chapin, F. S., Woodwell, G. M., Randerson, J. T., Rastetter, E. B., Lovett, G. M., Baldocchi, D. D., Clark, D. A., Harmon, M. E., Schimel, D. S., Valentini, R., Wirth, C., Aber, J. D., Cole, J. J., Goulden, M. L., Harden, J. W., Heimann, M., Howarth, R. W., Matson, P. A., McGuire, A. D., Melillo, J. M., Mooney, H. A., Neff, J. C., Houghton, R. A., Pace, M. L., Ryan, M. G., Running, S. W., Sala, O. E., Schlesinger, W. H.,

590   and Schulze, E. D.: Reconciling Carbon-cycle Concepts, Terminology, and Methods, Ecosystems, 9, 1041-1050, 2006.

Chemidlin Prévost-Bouré, N., Ngao, J., Berveiller, D., Bonal, D., Damesin, C., Dufrêne, E., Lata, J.-C., Le Dantec, V., Longdoz, B., Ponton, S., Soudani, K., and Epron, D.: Root exclusion through trenching does not affect the isotopic composition of soil CO2 efflux, Plant and Soil, 319, 1-13, 2008.

595 Chen, J., Luo, Y. Q., Xia, J. Y., Shi, Z., Jiang, L. F., Niu, S. L., Zhou, X. H., and Cao, J. J.: Differential responses of ecosystem respiration components to experimental warming in a meadow grassland on the Tibetan Plateau, Agricultural and Forest Meteorology, 220, 21-29, 2016.

Chen, J., Shi, W. Y., and Cao, J. J.: Effects of Grazing on Ecosystem CO2 Exchange in a Meadow Grassland on the Tibetan Plateau During the Growing Season, Environmental Management, 55, 347-359, 2015.

600 Chimner, R. A. and Cooper, D. J.: Influence of water table levels on CO2 emissions in a Colorado subalpine fen: an in situ microcosm study, Soil Biology and Biochemistry, 35, 345-351, 2003.

Chivers, M. R., Turetsky, M. R., Waddington, J. M., Harden, J. W., and McGuire, A. D.: Effects of Experimental Water Table and Temperature Manipulations on Ecosystem CO2 Fluxes in an Alaskan Rich Fen, Ecosystems, 12, 1329-1342, 2009.

605 Christiansen, J. R., Korhonen, J. F. J., Juszczak, R., Giebels, M., and Pihlatie, M.: Assessing the effects of chamber placement, manual sampling and headspace mixing on CH4 fluxes in a laboratory experiment, Plant and Soil, 343, 171-185, 2011.

Corradi, C., Kolle, O., Walter, K., Zimov, S. A., and Schulze, E. D.: Carbon dioxide and methane exchange of a north-east Siberian tussock tundra, Global Change Biology, 11, 1910-1925, 2005.

610 Diaz-Pines, E., Schindlbacher, A., Pfeffer, M., Jandl, R., Zechmeister-Boltenstern, S., and Rubio, A.: Root trenching: a useful tool to estimate autotrophic soil respiration? A case study in an Austrian mountain forest, European Journal of Forest Research, 129, 101-109, 2010.

Dorrepaal, E., Toet, S., van Logtestijn, R. S. P., Swart, E., van de Weg, M. J., Callaghan, T. V., and Aerts, R.: Carbon respiration from subsurface peat accelerated by climate warming in the subarctic, Nature, 460, 615   616-619, 2009.

Durbin, J. and Watson, G. S.: Testing for serial correlation in least squares regression, Biometrika, 37, 409-428, 1950.

Eckhardt, T. and Kutzbach, L.: MATLAB code to calculate gas fluxes from chamber-based methods. PANGAEA, 2016.

620 Elsgaard, L., Görres, C.-M., Hoffmann, C. C., Blicher-Mathiesen, G., Schelde, K., and Petersen, S. O.: Net ecosystem exchange of CO2 and carbon balance for eight temperate organic soils under agricultural management, Agriculture, Ecosystems & Environment, 162, 52-67, 2012.

Estop-Aragonés, C., Cooper, M. D., Fisher, J. P., Thierry, A., Garnett, M. H., Charman, D. J., Murton, J. B., Phoenix, G. K., Treharne, R., and Sanderson, N. K.: Limited release of previously-frozen C and increased 625   new peat formation after thaw in permafrost peatlands, Soil Biology and Biochemistry, 118, 115-129, 2018.

Frey, S. D., Drijber, R., Smith, H., and Melillo, J.: Microbial biomass, functional capacity, and community structure after 12 years of soil warming, Soil Biology & Biochemistry, 40, 2904-2907, 2008.

Gebauer, R. L. E., Reynolds, J. F., and Tenhunen, J. D.: Growth and allocation of the arctic sedges Eriophorum-630   Angustifolium and Eriophorum-Vaginatum - effects of variable soil oxygen and nutrient availability, Oecologia, 104, 330-339, 1995.

Görres, C. M., Kutzbach, L., and Elsgaard, L.: Comparative modeling of annual CO2 flux of temperate peat soils under permanent grassland management, Agriculture, Ecosystems & Environment, 186, 64-76, 2014.

Grogan, P. and Chapin, F. S.: Initial effects of experimental warming on above- and belowground components of 635   net ecosystem CO2 exchange in arctic tundra, Oecologia, 125, 512-520, 2000.

Grosse, G., Harden, J., Turetsky, M., McGuire, A. D., Camill, P., Tarnocai, C., Frolking, S., Schuur, E. A. G., Jorgenson, T., Marchenko, S., Romanovsky, V., Wickland, K. P., French, N., Waldrop, M., Bourgeau-Chavez, L., and Striegl, R. G.: Vulnerability of high-latitude soil organic carbon in North America to disturbance, Journal of Geophysical Research-Biogeosciences, 116, G00K06, 2011.

640 Hanson, P. J., Edwards, N. T., Garten, C. T., and Andrews, J. A.: Separating root and soil microbial contributions to soil respiration: A review of methods and observations, Biogeochemistry, 48, 115-146, 2000.

Harden, J. W., Koven, C. D., Ping, C.-L., Hugelius, G., David McGuire, A., Camill, P., Jorgenson, T., Kuhry, P., Michaelson, G. J., O'Donnell, J. A., Schuur, E. A. G., Tarnocai, C., Johnson, K., and Grosse, G.: Field information links permafrost carbon to physical vulnerabilities of thawing, Geophysical Research Letters, 645   39, 2012.

Harley, P. C., Tenhunen, J. D., Murray, K. J., and Beyers, J.: Irradiance and temperature effects on photosynthesis of tussock tundra Sphagnum mosses from the foothills of the Philip Smith Mountains, Alaska, Oecologia, 79, 251-259, 1989.

Heikkinen, J. E. P., Virtanen, T., Huttunen, J. T., Elsakov, V., and Martikainen, P. J.: Carbon balance in East 650   European tundra, Global Biogeochemical Cycles, 18, GB1023, 2004.

Helbig, M., Chasmer, L. E., Desai, A. R., Kljun, N., Quinton, W. L., and Sonnentag, O.: Direct and indirect climate change effects on carbon dioxide fluxes in a thawing boreal forest–wetland landscape, Global Change Biology, 23, 3231-3248, 2017.

Hicks Pries, C. E., Logtestijn, R. S., Schuur, E. A., Natali, S. M., Cornelissen, J. H., Aerts, R., and Dorrepaal, E.:
   Decadal warming causes a consistent and persistent shift from heterotrophic to autotrophic respiration in
   contrasting permafrost ecosystems, Global change biology, 21, 4508-4519, 2015.

Hicks Pries, C. E., Schuur, E. A., and Crummer, K. G.: Thawing permafrost increases old soil and autotrophic
   respiration in tundra: partitioning ecosystem respiration using delta (13)C and (14)C, Glob Chang Biol,
   19, 649-661, 2013.

Hobbie, S. E., Nadelhoffer, K. J., and Hogberg, P.: A synthesis: The role of nutrients as constraints on carbon
   balances in boreal and arctic regions, Plant and Soil, 242, 163-170, 2002.

Hugelius, G., Strauss, J., Zubrzycki, S., Harden, J. W., Schuur, E. A. G., Ping, C. L., Schirrmeister, L., Grosse, G.,
   Michaelson, G. J., Koven, C. D., O'Donnell, J. A., Elberling, B., Mishra, U., Camill, P., Yu, Z., Palmtag,
   J., and Kuhry, P.: Estimated stocks of circumpolar permafrost carbon with quantified uncertainty ranges
   and identified data gaps, Biogeosciences, 11, 6573-6593, 2014.

Jia, G. J., Epstein, H. E., and Walker, D. A.: Vegetation greening in the Canadian Arctic related to decadal
   warming, J Environ Monit, 11, 2231-2238, 2009.

Juszczak, R., Humphreys, E., Acosta, M., Michalak-Galczewska, M., Kayzer, D., and Olejnik, J.: Ecosystem
   respiration in a heterogeneous temperate peatland and its sensitivity to peat temperature and water table
   depth, Plant and Soil, 366, 505-520, 2013.

Kittler, F., Burjack, I., Corradi, C. A. R., Heimann, M., Kolle, O., Merbold, L., Zimov, N., Zimov, S., and Göckede,
   M.: Impacts of a decadal drainage disturbance on surface–atmosphere fluxes of carbon dioxide in a
   permafrost ecosystem, Biogeosciences, 13, 5315-5332, 2016.

Knoblauch, C., Beer, C., Liebner, S., Grigoriev, M. N., and Pfeiffer, E.-M.: Methane production as key to the
   greenhouse gas budget of thawing permafrost, Nature Climate Change, doi: 10.1038/s41558-018-0095-
   z, 2018. 2018.

Knoblauch, C., Beer, C., Sosnin, A., Wagner, D., and Pfeiffer, E. M.: Predicting long-term carbon mineralization
   and trace gas production from thawing permafrost of Northeast Siberia, Glob Chang Biol, 19, 1160-1172,
   2013.

Koskinen, M., Minkkinen, K., Ojanen, P., Kamarainen, M., Laurila, T., and Lohila, A.: Measurements of CO2
   exchange with an automated chamber system throughout the year: challenges in measuring night-time
   respiration on porous peat soil, Biogeosciences, 11, 347-363, 2014.

Kutzbach, L., Schneider, J., Sachs, T., Giebels, M., Nykanen, H., Shurpali, N. J., Martikainen, P. J., Alm, J., and
   Wilmking, M.: CO2 flux determination by closed-chamber methods can be seriously biased by
   inappropriate application of linear regression, Biogeosciences, 4, 1005-1025, 2007a.

Kutzbach, L., Wille, C., and Pfeiffer, E. M.: The exchange of carbon dioxide between wet arctic tundra and the
   atmosphere at the Lena River Delta, Northern Siberia, Biogeosciences, 4, 869-890, 2007b.

Kuzyakov, Y.: Sources of CO2 efflux from soil and review of partitioning methods, Soil Biology and
   Biochemistry, 38, 425-448, 2006.

Kwon, M. J., Heimann, M., Kolle, O., Luus, K. A., Schuur, E. A., Zimov, N., Zimov, S. A., and Göckede, M.:
   Long-term drainage reduces CO2 uptake and increases CO2 emission on a Siberian floodplain due to
   shifts in vegetation community and soil thermal characteristics, Biogeosciences, 13, 4219-4235, 2016.

Liebner, S., Zeyer, J., Wagner, D., Schubert, C., Pfeiffer, E.-M., and Knoblauch, C.: Methane oxidation associated
   with submerged brown mosses reduces methane emissions from Siberian polygonal tundra, Journal of
   Ecology, 99, 914-922, 2011.

Lynch, A. H., III, F. S. C., Hinzman, L. D., Wu, W., Lilly, E., Vourlitis, G., and Kim, E.: Surface Energy Balance
   on the Arctic Tundra: Measurements and Models, Journal of Climate, 12, 2585-2606, 1999.

Mahecha, M. D., Reichstein, M., Carvalhais, N., Lasslop, G., Lange, H., Seneviratne, S. I., Vargas, R., Ammann,
   C., Arain, M. A., Cescatti, A., Janssens, I. A., Migliavacca, M., Montagnani, L., and Richardson, A. D.:
   Global Convergence in the Temperature Sensitivity of Respiration at Ecosystem Level, Science, 329,
   838-840, 2010.

Marushchak, M. E., Kiepe, I., Biasi, C., Elsakov, V., Friborg, T., Johansson, T., Soegaard, H., Virtanen, T., and
   Martikainen, P. J.: Carbon dioxide balance of subarctic tundra from plot to regional scales,
   Biogeosciences, 10, 437-452, 2013.

McGuire, A. D., Anderson, L. G., Christensen, T. R., Dallimore, S., Guo, L. D., Hayes, D. J., Heimann, M.,
   Lorenson, T. D., Macdonald, R. W., and Roulet, N.: Sensitivity of the carbon cycle in the Arctic to climate
   change, Ecological Monographs, 79, 523-555, 2009.

McGuire, A. D., Christensen, T. R., Hayes, D., Heroult, A., Euskirchen, E., Kimball, J. S., Koven, C., Lafleur, P.,
   Miller, P. A., Oechel, W., Peylin, P., Williams, M., and Yi, Y.: An assessment of the carbon balance of
   Arctic tundra: comparisons among observations, process models, and atmospheric inversions,
   Biogeosciences, 9, 3185-3204, 2012.

Merbold, L., Kutsch, W. L., Corradi, C., Kolle, O., Rebmann, C., Stoy, P. C., Zimov, S. A., and Schulze, E. D.:
   Artificial drainage and associated carbon fluxes (CO2/CH4) in a tundra ecosystem, Global Change
   Biology, 15, 2599-2614, 2009.

715 Murray, K., Tenhunen, J., and Nowak, R.: Photoinhibition as a control on photosynthesis and production of Sphagnum mosses, Oecologia, 96, 200-207, 1993.

Muster, S., Langer, M., Heim, B., Westermann, S., and Boike, J.: Subpixel heterogeneity of ice-wedge polygonal tundra: a multi-scale analysis of land cover and evapotranspiration in the Lena River Delta, Siberia, Tellus B, 64, 17301, 2012.

720 Natali, S. M., Schuur, E. A. G., Trucco, C., Hicks Pries, C. E., Crummer, K. G., and Baron Lopez, A. F.: Effects of experimental warming of air, soil and permafrost on carbon balance in Alaskan tundra, Global Change Biology, 17, 1394-1407, 2011.

Nobrega, S. and Grogan, P.: Landscape and Ecosystem-Level Controls on Net Carbon Dioxide Exchange along a Natural Moisture Gradient in Canadian Low Arctic Tundra, Ecosystems, 11, 377-396, 2008.

725 Oechel, W. C., Vourlitis, G. L., Hastings, S. J., Ault, R. P., and Bryant, P.: The effects of water table manipulation and elevated temperature on the net CO2 flux of wet sedge tundra ecosystems, Global Change Biology, 4, 77-90, 1998.

Oechel, W. C., Vourlitis, G. L., Hastings, S. J., and Bochkarev, S. A.: Change in arctic CO2 flux over 2 decades - effects of climate-change at Barrow, Alaska, Ecological Applications, 5, 846-855, 1995.

730 Oechel, W. C., Vourlitis, G. L., Hastings, S. J., Zulueta, R. C., Hinzman, L., and Kane, D.: Acclimation of ecosystem CO2 exchange in the Alaskan Arctic in response to decadal climate warming, Nature, 406, 978-981, 2000.

Olivas, P. C., Oberbauer, S. F., Tweedie, C., Oechel, W. C., Lin, D., and Kuchy, A.: Effects of Fine-Scale Topography on CO2 Flux Components of Alaskan Coastal Plain Tundra: Response to Contrasting
735 Growing Seasons, Arctic, Antarctic, and Alpine Research, 43, 256-266, 2011.

Pihlatie, M. K., Christiansen, J. R., Aaltonen, H., Korhonen, J. F. J., Nordbo, A., Rasilo, T., Benanti, G., Giebels, M., Helmy, M., Sheehy, J., Jones, S., Juszczak, R., Klefoth, R., Lobo-do-Vale, R., Rosa, A. P., Schreiber, P., Serca, D., Vicca, S., Wolf, B., and Pumpanen, J.: Comparison of static chambers to measure CH4 emissions from soils, Agricultural and Forest Meteorology, 171, 124-136, 2013.

740 Romanovsky, V. E., Smith, S. L., and Christiansen, H. H.: Permafrost thermal state in the polar Northern Hemisphere during the international polar year 2007-2009: a synthesis, Permafrost and Periglacial Processes, 21, 106-116, 2010.

Runkle, B. R. K., Sachs, T., Wille, C., Pfeiffer, E. M., and Kutzbach, L.: Bulk partitioning the growing season net ecosystem exchange of CO2 in Siberian tundra reveals the seasonality of its carbon sequestration strength,
745 Biogeosciences, 10, 1337-1349, 2013.

Schneider, J., Kutzbach, L., and Wilmking, M.: Carbon dioxide exchange fluxes of a boreal peatland over a complete growing season, Komi Republic, NW Russia, Biogeochemistry, 111, 485-513, 2011.

Schuur, E. A., Vogel, J. G., Crummer, K. G., Lee, H., Sickman, J. O., and Osterkamp, T. E.: The effect of permafrost thaw on old carbon release and net carbon exchange from tundra, Nature, 459, 556-559, 2009.

750 Schuur, E. A. G., Abbott, B., and Permafrost Carbon, N.: High risk of permafrost thaw, Nature, 480, 32-33, 2011.

Schuur, E. A. G., Crummer, K. G., Vogel, J. G., and Mack, M. C.: Plant species composition and productivity following permafrost thaw and thermokarst in alaskan tundra, Ecosystems, 10, 280-292, 2007.

Schwamborn, G., Rachold, V., and Grigoriev, M. N.: Late Quaternary sedimentation history of the Lena Delta, Quaternary International, 89, 119-134, 2002.

755 Segal, A. D. and Sullivan, P. F.: Identifying the sources and uncertainties of ecosystem respiration in Arctic tussock tundra, Biogeochemistry, 121, 489-503, 2014.

Soegaard, H., Hasholt, B., Friborg, T., and Nordstroem, C.: Surface energy- and water balance in a high-arcticenvironment in NE Greenland, Theoretical and Applied Climatology, 70, 35-51, 2001.

Ström, L., Tagesson, T., Mastepanov, M., and Christensen, T. R.: Presence of Eriophorum scheuchzeri enhances
760 substrate availability and methane emission in an Arctic wetland, Soil Biology & Biochemistry, 45, 61-70, 2012.

Subke, J.-A., Inglima, I., and Francesca Cotrufo, M.: Trends and methodological impacts in soil CO2 efflux partitioning: A metaanalytical review, Global Change Biology, 12, 921-943, 2006.

Suseela, V., Conant, R. T., Wallenstein, M. D., and Dukes, J. S.: Effects of soil moisture on the temperature
765 sensitivity of heterotrophic respiration vary seasonally in an old-field climate change experiment, Global Change Biology, 18, 336-348, 2012.

Turetsky, M. R., Bond-Lamberty, B., Euskirchen, E., Talbot, J., Frolking, S., McGuire, A. D., and Tuittila, E. S.: The resilience and functional role of moss in boreal and arctic ecosystems, New Phytologist, 196, 49-67, 2012.

770 van't Hoff, J. H.: Lectures on theoretical and physical chemistry, Part 1: Chemical dynamics, Edward Arnold, London, 1898. 1898.

Virkkala, A.-M., Virtanen, T., Lehtonen, A., Rinne, J., and Luoto, M.: The current state of CO2 flux chamber studies in the Arctic tundra: a review, Progress in Physical Geography: Earth and Environment, doi: 10.1177/0309133317745784, 2017. 0309133317745784, 2017.

775 Voigt, C., Lamprecht, R. E., Marushchak, M. E., Lind, S. E., Novakovskiy, A., Aurela, M., Martikainen, P. J., and
Biasi, C.: Warming of subarctic tundra increases emissions of all three important greenhouse gases–
carbon dioxide, methane, and nitrous oxide, Global change biology, 2016. 2016.
Vourlitis, G. L., Oechel, W. C., Hope, A., Stow, D., Boynton, B., Verfaillie, J., Zulueta, R., and Hastings, S. J.:
Physiological models for scaling plot measurements of CO2 flux across an arctic tundra landscape,
780 Ecological Applications, 10, 60-72, 2000.
Walker, D. A., Raynolds, M. K., Daniëls, F. J. A., Einarsson, E., Elvebakk, A., Gould, W. A., Katenin, A. E.,
Kholod, S. S., Markon, C. J., Melnikov, E. S., Moskalenko, N. G., Talbot, S. S., Yurtsev, B. A., and
Franklin, J.: The Circumpolar Arctic vegetation map, Journal of Vegetation Science, 16, 267-282, 2005.
Walz, J., Knoblauch, C., Böhme, L., and Pfeiffer, E.-M.: Regulation of soil organic matter decomposition in
785 permafrost-affected Siberian tundra soils - Impact of oxygen availability, freezing and thawing,
temperature, and labile organic matter, Soil Biology and Biochemistry, 110, 34-43, 2017.
Wilber, A. C., Kratz, D. P., and Gupta, S. K.: Surface emissivity maps for use in satellite retrievals of longwave
radiation, 1999. 1999.
Wille, C., Kutzbach, L., Sachs, T., Wagner, D., and Pfeiffer, E.-M.: Methane emission from Siberian arctic
790 polygonal tundra: eddy covariance measurements and modeling, Global Change Biology, 14, 1395-1408,
2008.
WRB, I. W. G.: World reference base for soil resources 2014 international soil classification system for naming
soils and creating legends for soil maps, FAO, Rome, 2014.
Yershov, E. D.: General Geocryology, Cambridge University Press, Cambridge, 1998.
795 Zamolodchikov, D., Karelin, D., and Ivaschenko, A.: Sensitivity of tundra carbon balance to ambient temperature,
Water, Air and Soil Pollution, 119, 157-169, 2000.
Zimov, S. A., Davydov, S. P., Zimova, G. M., Davydova, A. I., Schuur, E. A. G., Dutta, K., and Chapin, F. S.:
Permafrost carbon: Stock and decomposability of a globally significant carbon pool, Geophysical
Research Letters, 33, L20502, 2006a.
800 Zimov, S. A., Schuur, E. A., and Chapin, F. S.: Permafrost and the global carbon budget, Science, 312, 1612-1613,
2006b.
Zona, D., Lipson, D. A., Richards, J. H., Phoenix, G. K., Liljedahl, A. K., Ueyama, M., Sturtevant, C. S., and
Oechel, W. C.: Delayed responses of an Arctic ecosystem to an extreme summer: impacts on net
ecosystem exchange and vegetation functioning, Biogeosciences, 11, 5877-5888, 2014.
805 Zona, D., Oechel, W. C., Richards, J. H., Hastings, S., Kopetz, I., Ikawa, H., and Oberbauer, S.: Light-stress
avoidance mechanisms in a Sphagnum-dominated wet coastal Arctic tundra ecosystem in Alaska,
Ecology, 92, 633-644, 2011.
Zubrzycki, S., Kutzbach, L., Grosse, G., Desyatkin, A., and Pfeiffer, E. M.: Organic carbon and total nitrogen
stocks in soils of the Lena River Delta, Biogeosciences, 10, 3507-3524, 2013.

810

Table 1 – Means and range of the modelled fluxes in µg CO_2 m^{-2} s^{-1}.

		polygon center	polygon rim
		in µg CO_2 m^{-2} s^{-1}	*in µg CO_2 m^{-2} s^{-1}*
NEE	mean	-68 ± 12	-26 ± 19
	range	-288 ± 53 to 54 ± 2	-117 ± 60 to 49 ± 10
GPP	mean	-98 ± 10	-61 ± 17
	range	up to -342 ± 53	up to -163 ± 57
R_{eco}	mean	29 ± 11	35 ± 9
	range	12 ± 3 to 69 ± 7	21 ± 3 to 77 ± 14
R_H	mean	11 ± 3	21 ± 5
	range	6 ± 1 to 27 ± 2	14 ± 4 to 46 ± 13
R_A	mean	19 ± 11	14 ± 5
	range	1 ± 3 to 55 ± 4	5 ± 5 to 32 ± 19
NPP	mean	-85 ± 12	-49 ± 20
	range	up to -300 ± 53	up to -142 ± 57

Table 2 - Comparison of daily averaged CO_2 fluxes from different arctic tundra sites, which are comparable in vegetation and soil composition to our study site. All listed fluxes were measured with the closed chamber technique.

Location	Tundra type	Period	NEE (g C m^{-2} d^{-1})	GPP (g C m^{-2} d^{-1})	R$_{eco}$ (g C m^{-2} d^{-1})	Ref
Lena River Delta, RU (72°N,127°E)	*pol. rim*	*Jul-Sep 2015*	*-0.6 ± 0.4*	*-1.4 ± 0.4*	*0.8 ± 0.2*	*a*
	pol. center		*-1.6 ± 0.3*	*-2.3 ± 0.2*	*0.7 ± 0.1*	
Lek Vorkuta, RU (67°N, 63°E)	shrub	Jul-Aug 1996	-0.6 ± 0.3	-4.5 ± 0.4	3.9 ± 0.3	b
	sedge bog		-1.0 ± 0.2	-3.2 ± 0.4	2.2 ± 0.3	
Prudhoe Bay, US (70°N, 149°W)	pol. tundra	Jun-Aug 1994	-0.6 ± 0.4	-5.2 ± 0.6	4.6 ± 0.3	c
Lek Vorkuta, RU (67°N, 63°E)	wet peaty tundra	Jun-Sep 2001	-1.1 ± 0.2	-1.9 ± 0.2[*]	0.9 ± 0.2[*]	d
Daring Lake, CA (65°N, 111°W)	dry heath	Jun-Sep 2004	-0.01 ± 0.1	-1.7 ± 0.3	1.8 ± 0.2	e
	mesic birch		-0.4 ± 0.3	-3.2 ± 0.5	2.8 ± 0.3	
	wet sedge		-0.9 ± 0.1	-1.7 ± 0.1	0.8 ± 0.1	
Barrow, US (71°N, 157°W)	pol. rim	Jun-Aug 2005	-0.1 ± 0.5	-3.7 ± 0.2	3.6 ± 0.3	f
	pol. center		-0.2 ± 0.2	-3.1 ± 0.1	2.9 ± 0.1	
	pol. rim	Jun-Aug 2006	-0.7 ± 0.2	-3.1 ± 0.3	2.4 ± 0.2	
	pol. center		-0.8 ± 0.2	-2.3 ± 0.2	1.5 ± 0.2	
Barrow, US (71°N, 157°W)	pol. center	Jun-Aug 1992	0.04 ± 0.05	-0.8 ± 0.1	0.8 ± 0.1	g
Zackenberg, GL (74°N, 20°W)	sedge-dom. fen	Jun-Aug	-2.6 ± 0.3	-5.6 ± 0.4	3.0 ± 0.1	h

a: this study; b: Zamolodchikov et al. (2000); c: Vourlitis et al. (2000); d: Heikkinen et al. (2004); e: Nobrega and Grogan (2008); f: Olivas et al. (2011); g: Oechel et al. (1995); h: Ström et al. (2012)
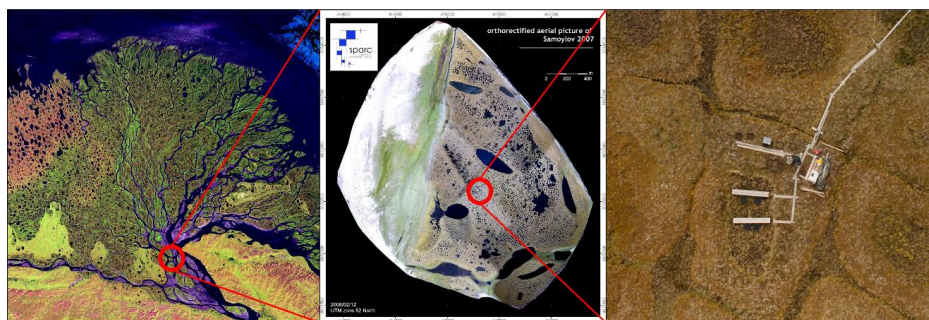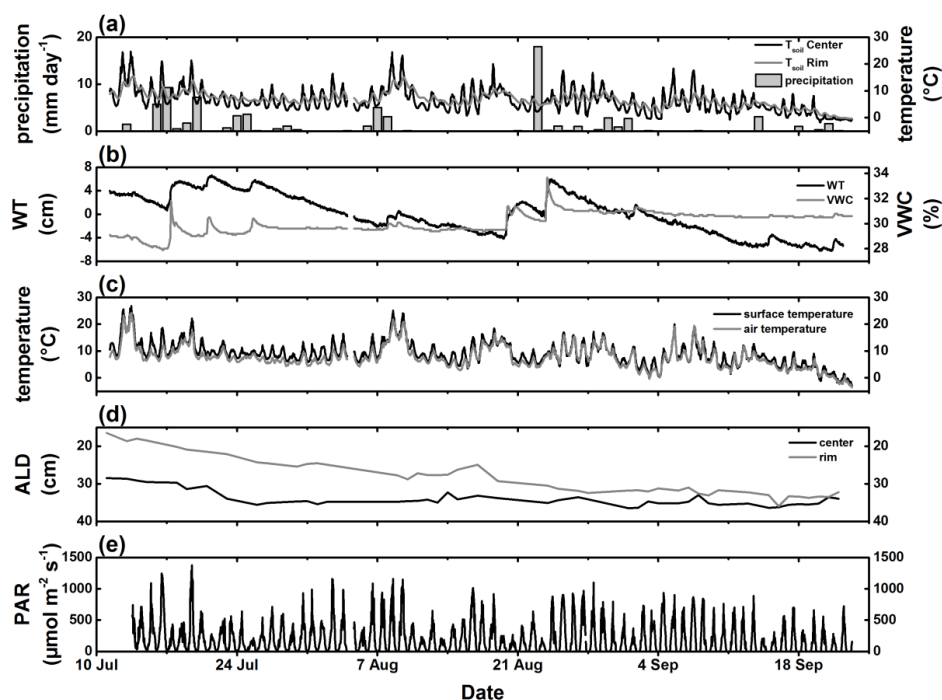*: standard deviation estimated

Figure 1 - The study site on Samoylov Island, Lena River Delta in Northeastern Siberia (72°22'N, 126°28'E). (Satellite images – left: NASA Landsat Programme: Lena Delta in Landsat 7; available at: http://earthobservatory.nasa.gov/IOTD/view.php?id=2704, 2002; middle: Boike et al. (2012); right: Boike et al. (2015)

825   **Figure 2 - Meteorological conditions from mid of July to end September. Panel (a) soil temperatures measured at 2 cm depth at the rim and center microsite and daily precipitation measured at the eddy covariance tower; (b) water table relative to the soil surface measured at the polygon center and volumetric water content measured at the polygon rim; (c) Half-hourly air temperature measured at 2 m height at the eddy covariance tower and surface temperature; (d) daily measured thaw depth at the polygon rim an center; (e) photosynthetically active radiation (PAR) measured half-hourly**
830   **at the eddy covariance tower.**

Figure 3 - Chamber measured NEE, R_{eco} and R_H fluxes as well as calculated GPP, NPP and R_A fluxes. The error bars denote the standard deviation of the four replicate measurements at each microsite. Panel (a) fluxes of NEE (n = 83), R_{eco} (n = 85) and R_H (n = 85) at the polygon center; (b) calculated fluxes of GPP (n = 83), NPP (n = 83) and R_A (n = 85) at the polygon center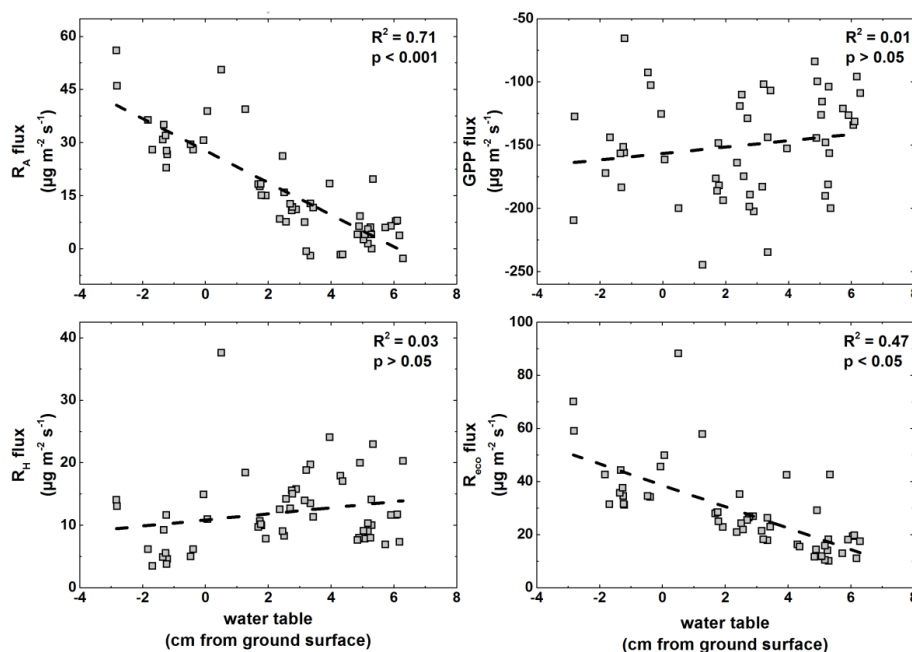; panel (c) measured fluxes of NEE (n = 83), R_{eco} (n = 85) and R_H (n = 85) at the polygon rim; (d) calculated fluxes of GPP (n = 83), NPP (n = 83) and R_A (n = 85) at the polygon rim.

Figure 4 - Relationships between water table fluctuations and (a) R_{eco} fluxes, (b) R_H fluxes, (c) R_A fluxes and (d) GPP fluxes during the period July-August at the polygon center. Negative values on the x-axis indicate a water table below the soil surface.
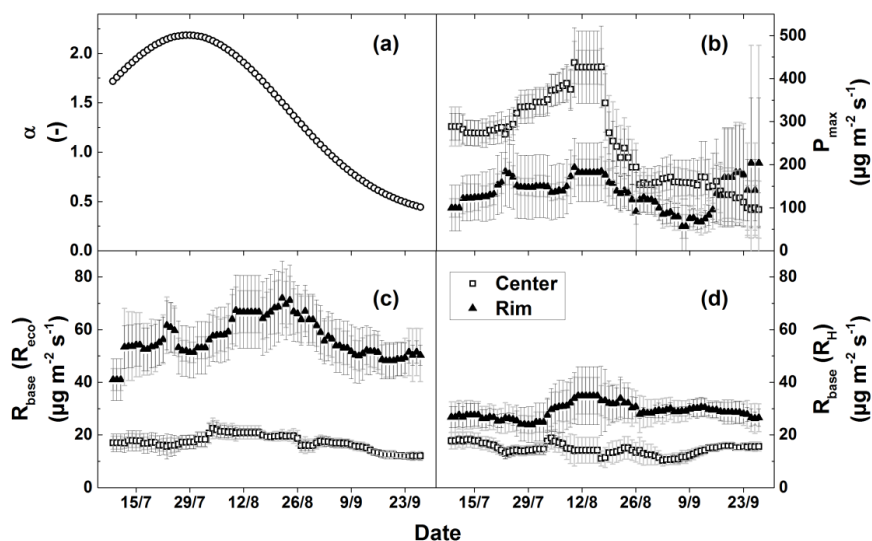
Figure 5 - Fitting parameters of the fitted CO₂ flux models. The values are given with the standard deviation of the model results from the single measurement plots (light grey error bars) and the confidence intervals (95%) of the fitting parameters (dark grey error bars).
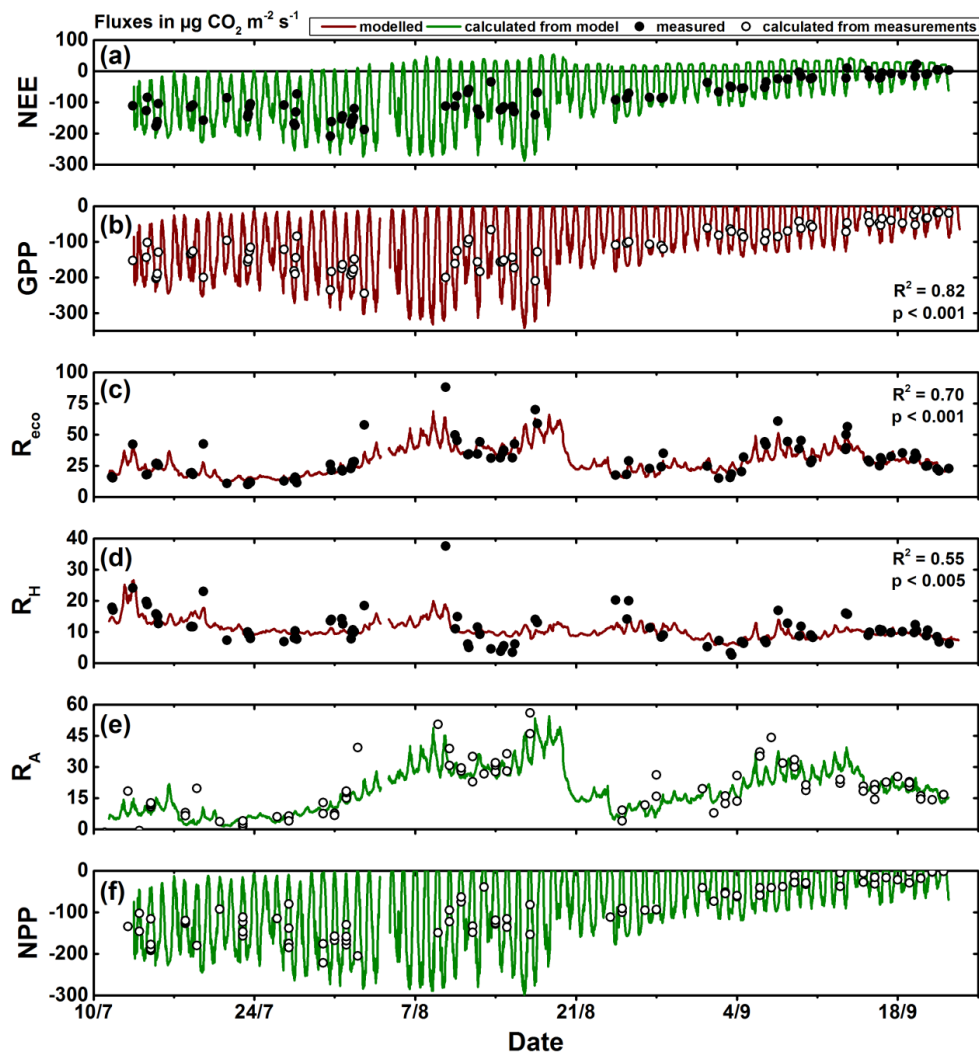
845

Figure 6 - Modelled and measured CO₂ fluxes at the polygon center. Measured fluxes are available for NEE, R$_{eco}$ and R$_H$. NEE model fluxes were calculated from modelled GPP minus modelled R$_{eco}$, R$_A$ model fluxes from modelled R$_{eco}$ minus modelled R$_H$ and NPP model fluxes from modelled GPP minus modelled R$_A$. Note the different scales of the y-axes.
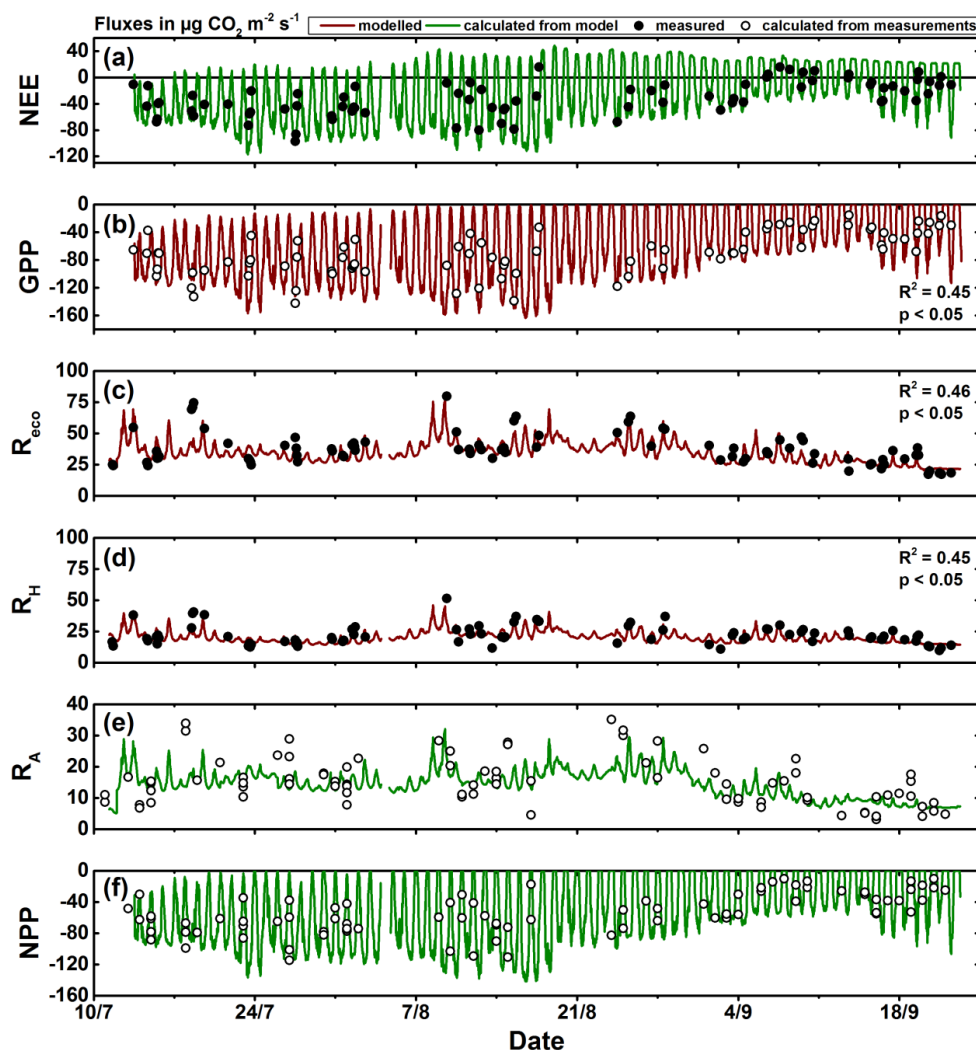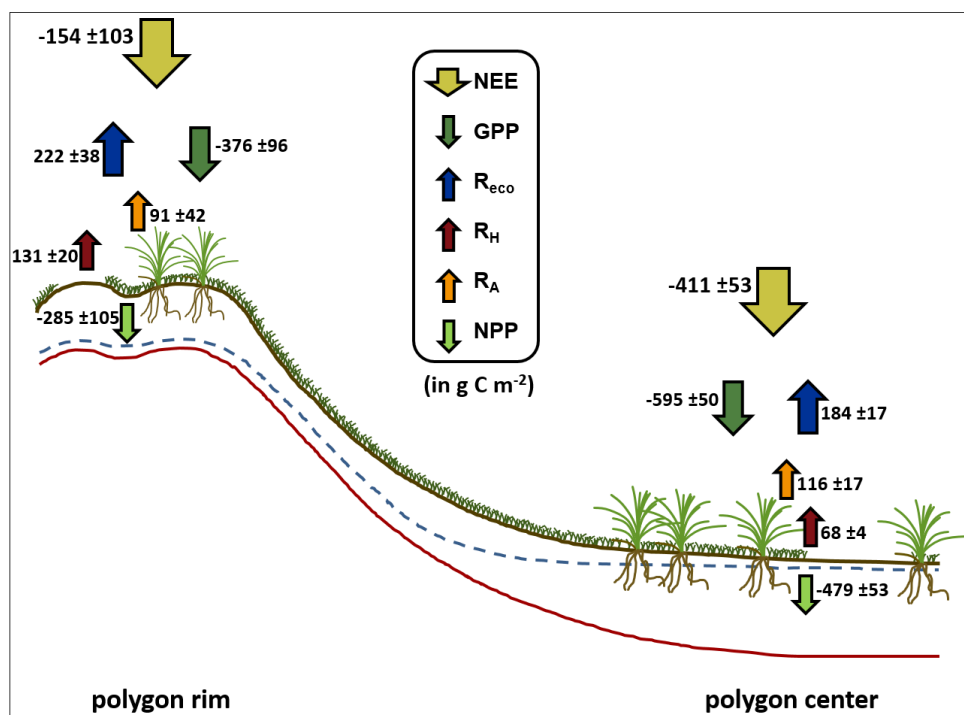
850

Figure 7 - Modelled and measured CO₂ fluxes at the polygon rim. Measured fluxes are available for NEE, R_{eco} and R_H. NEE model fluxes were calculated from modelled GPP minus modelled R_{eco}, R_A model fluxes from modelled R_{eco} minus modelled R_H and NPP model fluxes from modelled GPP minus modelled R_A. Note the different scales of the y-axes.

855

Figure 8 – Integrated CO₂ fluxes at the polygon rim and center. The values were calculated from the model results and are given in g C m⁻². In total, both microsites acted as a net CO₂ sink during the growing season. NEE= net ecosystem exchange; GPP= gross primary productivity; R$_{eco}$= ecosystem respiration; R$_H$= heterotrophic respiration; R$_A$= autotrophic respiration and NPP= net primary productivity.